Transient-time correlation function applied to mixed shear and elongational flows

Remco Hartkamp, Stefano Bernardi, and B. D. Todd

Citation: J. Chem. Phys. **136**, 064105 (2012); doi: 10.1063/1.3684753
View online: http://dx.doi.org/10.1063/1.3684753
View Table of Contents: http://jcp.aip.org/resource/1/JCPSA6/v136/i6
Published by the American Institute of Physics.

Transient-time correlation function applied to mixed shear and elongational flows

Remco Hartkamp,[1,a)] Stefano Bernardi,[2,b)] and B. D. Todd[3,c)]
[1]*Multi Scale Mechanics, MESA+ Institute for Nanotechnology, University of Twente, P.O. Box 217, 7500 AE Enschede, The Netherlands*
[2]*Queensland Micro- and Nanotechnology Centre, School of Biomolecular and Physical Sciences, Griffith University, Brisbane, Queensland 4111, Australia*
[3]*Mathematics Discipline, Faculty of Engineering and Industrial Sciences and Centre for Molecular Simulation, Swinburne University of Technology, Hawthorn, Victoria 3122, Australia*

(Received 8 December 2011; accepted 24 January 2012; published online 10 February 2012)

The transient-time correlation function (TTCF) method is used to calculate the nonlinear response of a homogeneous atomic fluid close to equilibrium. The TTCF response of the pressure tensor subjected to a time-independent planar mixed flow of shear and elongation is compared to directly averaged non-equilibrium molecular dynamics (NEMD) simulations. We discuss the consequence of noise in simulations with a small rate of deformation. The generalized viscosity for planar mixed flow is also calculated with TTCF. We find that for small rates of deformation, TTCF is far more efficient than direct averages of NEMD simulations. Therefore, TTCF can be applied to fluids with deformation rates which are much smaller than those commonly used in NEMD simulations. Ultimately, TTCF applied to molecular systems is amenable to direct comparison between NEMD simulations and experiments and so in principle can be used to study the rheology of polymer melts in industrial processes. © *2012 American Institute of Physics*. [doi:10.1063/1.3684753]

I. INTRODUCTION

The SLLOD algorithm for homogeneous shear flow[1,2] is a well-known non-equilibrium molecular dynamics (NEMD) method to simulate homogeneous atomic or molecular shear flow. It has also been proven to be applicable to any generalized homogeneous flow, including elongational flow and mixed flow.[3,4] In combination with Lees-Edwards periodic boundary conditions,[5] indefinitely long simulations can be conducted for shear. The 1990s has seen the development of methods to simulate indefinitely long extensional flow by applying the Kraynik and Reinelt[6] periodic boundary conditions.[7–9] Shear or elongational flow simulations have proven to be useful in understanding processes, such as extrusion, injection molding, sheet casting, and the dynamics of DNA chains. These, and many other industrial and biological processes are in reality much more complicated.[10,11] Hunt *et al.*[12] recently devised an algorithm with which any linear combination of shear and planar elongational flow, called planar mixed flow (PMF), can be simulated. They engineered a set of periodic boundary conditions, based on lattice theory, that allows for indefinitely long simulations. This new algorithm decreases the gap between NEMD simulations and real systems.

In a steady state, one can average NEMD simulations over time to eliminate the fluctuations related to instantaneous quantities. This approach is efficient far from equilibrium, where the signal-to-noise ratio is high. Close to equilibrium, however, very long time-averages are needed in order to obtain good statistics, making this method unfeasible for simulations with very small deformation rates. Molecular dynamics simulations are typically run at fields that are at least four orders of magnitude larger than in typical experiments, and thus not very suitable for mimicking experiments on a one-to-one basis. However, techniques such as temperature-time superposition[13] can be used to directly relate NEMD results to experiments, confirming the high accuracy of such simulations. Bair *et al.*[14] have applied this method successfully to compare NEMD shear flow simulations of low-molecular-weight fluids to experimental data. The transient-time correlation function (TTCF) (Refs. 2, 15, and 16) method offers a more efficient way to study the rheology of fluids close to equilibrium. This method is based on the time-correlation between the initial rate of energy dissipation and the transient response after an external field is activated.

While atomic fluids may behave as a Newtonian fluid even for fields that are larger than industrial applications, for complex fluids, the nonlinear response can dominate already at very small external fields. Therefore, a nonlinear-response treatment, such as TTCF, is very important. For example, Pan and McCabe,[17] and later Mazyar *et al.*,[18] have applied TTCF to calculate the viscosity of *n*-decane in a homogeneous shear flow. The transient response of shear flow[1,19–22] and various types of shear-free flow[23,24] have been studied in the past for various types of atomic systems. Here, we consider the transient response of atomic PMF.

In Sec. II, we give a derivation of the transient-time correlation function and discuss the consequences of instantaneous fluctuations on the accuracy of the calculation. In Sec. III, we treat a set of equations of motion for a homogeneous mixed flow of shear and elongation. In Sec. IV, we discuss

a)Electronic mail: r.m.hartkamp@utwente.nl.
b)Electronic mail: s.bernardi@griffith.edu.au.
c)Electronic mail: btodd@swin.edu.au.

the simulation details and implications of phase-space mapping. In Sec. V, we discuss the simulation results for four field strengths and finally we end with some concluding comments in Sec. VI.

II. TRANSIENT-TIME CORRELATION FUNCTION

Evans and Morriss[1,19,20,25,26] described the procedure for TTCF in a number of papers. Here, we briefly follow the procedure for the general case. The evolution of a field-dependent phase variable B (which is denoted as a scalar here, but can be a tensor as well) subject to a homogeneous external field (activated at $t = 0$) can be given by the time-derivative of the Heisenberg representation of a phase-space average

$$\frac{d\langle B(t)\rangle}{dt} = \int d\mathbf{\Gamma}\, f(0)\dot{\mathbf{\Gamma}} \cdot \frac{\partial B(t)}{\partial \mathbf{\Gamma}}, \tag{1}$$

where $f(0)$ is the N-particle distribution function at time zero (i.e., just before the external field is turned on) and $\mathbf{\Gamma}$ is the phase-space vector. The phase variable is propagated via the phase variable propagator $\exp(\mathrm{iL}t)$, which relates the current value of a phase variable to the initial value via $B(t) = \exp(\mathrm{iL}t)B(0)$, where iL is the p-Liouvillean. This implies that the current value of the phase variable depends only on the initial value and on the equations of motion and not on the current phase-space vector.

Integrating Eq. (1) by parts gives

$$\frac{d\langle B(t)\rangle}{dt} = [f(0)\dot{\mathbf{\Gamma}}B(t)]_S - \int d\mathbf{\Gamma}\, B(t)\frac{\partial}{\partial \mathbf{\Gamma}} \cdot (f(0)\dot{\mathbf{\Gamma}}), \tag{2}$$

where the surface term is zero. Integrating Eq. (2) with respect to time gives

$$\langle B(t)\rangle = \langle B(0)\rangle - \int_0^t ds \int d\mathbf{\Gamma}\, B(s)\frac{\partial}{\partial \mathbf{\Gamma}} \cdot (f(0)\dot{\mathbf{\Gamma}}). \tag{3}$$

For the adiabatic case, Eq. (3) can be rewritten using[23]

$$\frac{\partial}{\partial \mathbf{\Gamma}} \cdot (f(0)\dot{\mathbf{\Gamma}}) = i\mathcal{L}f(0) = \beta \mathbf{J}(0) : \mathbf{F}_e f(0) = \beta V(\mathbf{P}(0) : \nabla \mathbf{u}) f(0) = -\beta \dot{\mathcal{H}}^{ad}(0) f(0), \tag{4}$$

where $i\mathcal{L}$ is the f-Liouvillean, $\beta = 1/\mathrm{k_B}T$, $\mathbf{J}(0)$ is the initial dissipative flux, $\mathbf{F}_e$ is the external driving force, and $\dot{\mathcal{H}}^{ad}(0) = -V(\mathbf{P}(0) : \nabla \mathbf{u})$ is the rate of energy dissipation of the adiabatic system the instant the field is turned on. The rate of energy dissipation can be calculated from the SLLOD equations of motion (Eqs. (11) and (12)) presented in Sec. III. Substituting Eq. (4) into Eq. (3) results in the TTCF formulation for a general homogeneous flow

$$\langle B(t)\rangle = \langle B(0)\rangle - \beta V \int_0^t ds\, \langle B(s)(\mathbf{P}(0) : \nabla \mathbf{u})\rangle, \tag{5}$$

$$= \langle B(0)\rangle + \int_0^t ds\, \langle B(s)\Omega(0)\rangle, \tag{6}$$

where $\Omega(0) \equiv -\beta V \mathbf{P}(0) : \nabla \mathbf{u}$.

If the system exhibits mixing,[20] then the instantaneous phase variable $B(t)$ becomes uncorrelated to the initial rate of energy dissipation $\mathbf{P}(0) : \nabla \mathbf{u}$ for large t, leading to $\langle B(t)\Omega(0)\rangle \sim \langle B(t)\rangle\langle\Omega(0)\rangle$. The ensemble average of the initial rate of energy dissipation $\langle\Omega(0)\rangle$ approaches zero in the statistical limit for infinitely many trajectories or atoms. However, due to numerical inaccuracy $\langle B(t)\rangle\langle\Omega(0)\rangle \neq 0$ (this can be seen as the rate of growth of the error due to an initial non-zero average rate of energy dissipation) and thus the integral never converges to a constant value. In order to account for this numerical inaccuracy, we can subtract the error as follows:

$$\langle B(s)(\Omega(0) - \langle\Omega(0)\rangle)\rangle = \langle B(s)\Omega(0)\rangle - \langle B(s)\rangle\langle\Omega(0)\rangle, \tag{7}$$

$$= \langle (B(s) - \langle B(s)\rangle)\Omega(0)\rangle, \tag{8}$$

$$= \langle \Delta B(s)\Omega(0)\rangle, \tag{9}$$

where $\Delta B(s) = B(s) - \langle B(s)\rangle$ denotes the instantaneous fluctuations in $B(s)$. Note that this expression goes to zero when $B(t)$ and $\Omega(0)$ become uncorrelated.

In the special case that the initial average rate of energy dissipation $\langle\Omega(0)\rangle$ is exactly zero, the correlation can be rewritten to $\langle B(s)\Omega(0)\rangle = \langle \Delta B(s)\Omega(0)\rangle$. This condition is only exactly satisfied in the case of a suitable phase-space mapping, which will be discussed in Sec. IV.

Substituting the corrected correlation function (Eq. (9)) into Eq. (5) gives

$$\langle B(t)\rangle = \langle B(0)\rangle - \beta V \int_0^t ds\, \langle \Delta B(s)\Omega(0)\rangle, \tag{10}$$

which is, in general, not identical to Eq. (6).

III. PLANAR MIXED FLOW

NEMD simulations are a commonly used tool to study the rheology of homogeneous fluids out of equilibrium.[4,27] The SLLOD equations of motion[2,3] are a set of first-order linear differential equations that couple an external driving force to a fluid

$$\dot{\mathbf{r}}_i = \frac{\mathbf{p}_i}{m_i} + \mathbf{r}_i \cdot \nabla \mathbf{u}, \tag{11}$$

$$\dot{\mathbf{p}}_i = \mathbf{F}_i^{\phi} - \mathbf{p}_i \cdot \nabla \mathbf{u} - \zeta \mathbf{p}_i. \tag{12}$$

The first equation represents the evolution of the position of atom i, where $\mathbf{r}$ is the position, $\mathbf{p}$ is the peculiar momentum, and $\nabla \mathbf{u}$ is the velocity gradient. The velocity gradient contains the homogeneous external field that drives the system away from a thermodynamic equilibrium. Equation (11) decomposes the velocity into a thermal velocity $\mathbf{c}_i = \mathbf{p}_i/m_i$ and the local streaming velocity $\mathbf{u}(\mathbf{r}_i) = \mathbf{r}_i \cdot \nabla \mathbf{u}$. The type of flow is a direct consequence of the velocity gradient. The second equation gives the evolution of the peculiar momentum. The force on atom i due to other atoms is denoted by $\mathbf{F}_i^{\phi}$. The last term in Eq. (12) couples the fluid to a heat bath, where ζ is a thermostat variable, which can be seen as a friction coefficient. The thermostat adds or removes heat in order to control the kinetic temperature.

In the past, mainly shear flow[1,21,22,28–30] and elongational flow[7,9,23,24,29,31–35] have been studied due to their relative

simplicity. Evans and Heyes[36] were the first to combine shear and elongation. Their simulations were however limited by the deformation of the cell size in the direction of contraction since suitable periodic boundary conditions (that allow for indefinitely long simulations) were not available. Recently, Hunt *et al.*[12] devised an algorithm to simulate indefinite duration PMF using NEMD methods. The constant, traceless velocity gradient tensor is given by

$$\nabla \mathbf{u} = \begin{bmatrix} \dot{\epsilon} & 0 & 0 \\ \dot{\gamma} & -\dot{\epsilon} & 0 \\ 0 & 0 & 0 \end{bmatrix}, \tag{13}$$

where $\dot{\epsilon}$ is the rate of extension and $\dot{\gamma}$ is the shear rate. Expansion is applied in the x-direction and contraction in y. Shear is applied in the x-y plane, with the gradient of velocity in y.

Substituting Eq. (13) into the SLLOD equations of motion (Eqs. (11) and (12)), the equations under which planar mixed flow evolves become

$$\dot{\mathbf{r}}_i = \frac{\mathbf{p}_i}{m_i} + \dot{\epsilon}(x_i \mathbf{e}_x - y_i \mathbf{e}_y) + \dot{\gamma} y_i \mathbf{e}_x, \tag{14}$$

$$\dot{\mathbf{p}}_i = \mathbf{F}_i^{\phi} - \dot{\epsilon}(p_{xi} \mathbf{e}_x - p_{yi} \mathbf{e}_y) - \dot{\gamma} p_{yi} \mathbf{e}_x - \zeta \mathbf{p}_i, \tag{15}$$

where $\mathbf{e}_\alpha$ is a unit vector oriented in the α-direction, α_i is the position of atom i, and $p_{\alpha i}$ is its peculiar momentum in the α-direction. Each atom feels the external field at the same time. The explicit external field in combination with the homogeneous character makes the SLLOD equations of motion amenable to response theory.

Combining the TTCF formulation (Eq. (10)) with the rate of energy dissipation (Eq. (4)) and the velocity gradient for PMF (Eq. (13)), results in the nonlinear response of a phase variable B that evolves under PMF

$$\langle B(t) \rangle = \langle B(0) \rangle - \beta V \left(\dot{\epsilon} \int_0^t ds \, \langle \Delta B(s)(P_{xx}(0) - P_{yy}(0)) \rangle \right.$$
$$\left. + \dot{\gamma} \int_0^t ds \, \langle \Delta B(s) P_{xy}(0) \rangle \right). \tag{16}$$

The nonlinear response of observable $B(t)$ evolving under PMF will, in general, not be the same as the superposition of the nonlinear response of separate planar shear and planar elongation simulations. The reason for this is that the nonlinear response contains the product of the instantaneous phase variable $B(t)$ (evolving under PMF), as well as the initial dissipation Ω for PMF. Since both quantities are field-dependent, the product does not simply relate to the field in a linear fashion. For the linear response, the superposition would be valid, since the dissipation for PMF is simply a linear combination of that of planar Couette flow and planar elongational flow (PEF) and the non-equilibrium (field-dependent) values of the phase variable are not included in the linear response formulation.

IV. SIMULATIONS

We simulate an atomic fluid whose interactions are mediated via a Weeks-Chandler-Andersen (WCA) (Ref. 37) potential and the equations of motion are integrated with a fourth-order Runge-Kutta scheme with a time-step of $\Delta t = 0.001$. This algorithm is self-starting, which is an important property for the study of transient behavior.[20] All physical quantities presented are reduced using the particle mass m, interaction length scale σ, and the potential energy well-depth ϵ. These scales are set to unity. The phase point of the fluid is set close to the Lennard-Jones triple point, $\rho = 0.8442$ and $T = 0.772$, where the properties of simple fluids (such as Argon) are well-known. To maintain a constant temperature, the generated heat needs to be removed from the system. This is done via the Gaussian isokinetic thermostat.[38]

The initial cell vectors in the plane of deformation have lengths 14.43 and 8.43 and a relative angle of 90° (for our simulation with equal rates of shear and elongational). As time advances, the simulation cell is deformed. Since the cell size has to be at least twice the cut-off distance of the potential ($2^{1/6}$ for the WCA potential) in each direction (in order for atoms not to interact with their periodic image), the maximum simulation time would be limited by the cell size in the contraction direction, regardless of the initial cell-size. Hunt *et al.*[12] introduced a set of boundary conditions that remap the positions of the atoms to the initial simulation cell after a certain time without disturbing the flow. These boundary conditions avoid the time limit due to the deformation of the cell and allow for indefinitely long simulations.

Before the external field is activated and the transient response can be calculated, the simulation is relaxed to equilibrium. This results in an initial state for a non-equilibrium simulation $\mathbf{\Gamma}_1 = (\mathbf{x}, \mathbf{y}, \mathbf{z}, \mathbf{p}_x, \mathbf{p}_y, \mathbf{p}_z)$, where each component is a vector with length N. If a system exhibits mixing, we can modify the initial state in specific ways, such that another initial state is created with equal probability and internal energy. This procedure is called phase-space mapping.[2,19] The phase-space mapping provides additional initial configurations with the purpose of creating more field-dependent trajectories from an equilibrium phase point. These additional trajectories enhance the statistical accuracy.

If a mapping can be created that exactly satisfies $\sum_M (\mathbf{P}(\mathbf{\Gamma}_M(0)) : \nabla \mathbf{u}) = 0$ (where the summation is over the non-equilibrium starting states), the phase-space mapping eliminates the numerical uncertainty that leads to a non-zero initial rate of energy dissipation.[19] Hence, $\langle \Omega(0) \rangle = 0$ would be exactly satisfied, making the subtraction shown in Eq. (7) redundant. If the pressure tensor is symmetric at time $t = 0$ (before the field is activated), the phase vector $\mathbf{\Gamma}_M = M^{PMF}(\mathbf{\Gamma}_1) = (-\mathbf{y}, \mathbf{x}, \mathbf{z}, -\mathbf{p}_y, \mathbf{p}_x, \mathbf{p}_z)$ satisfies the condition given above for PMF. The off-diagonal pressure term P_{xy} is mapped to $-P_{yx}$, which cancel out against each other in the sum over the non-equilibrium starting states in the case that $P_{xy}(0) = P_{yx}(0)$. The pressure tensor for an atomic fluid is inherently symmetric. This is, however, not always the case for molecular fluids, in which case an additional phase-space mapping is required. In addition to satisfying this condition, a suitable phase-space mapping should not conflict with the boundary conditions. Since boundary conditions for a generic flow type do not exist that will guarantee indefinite simulation times, the phase-space mapping needs to be addressed on a case-to-case basis. Indefinite simulations of PMF, in general,

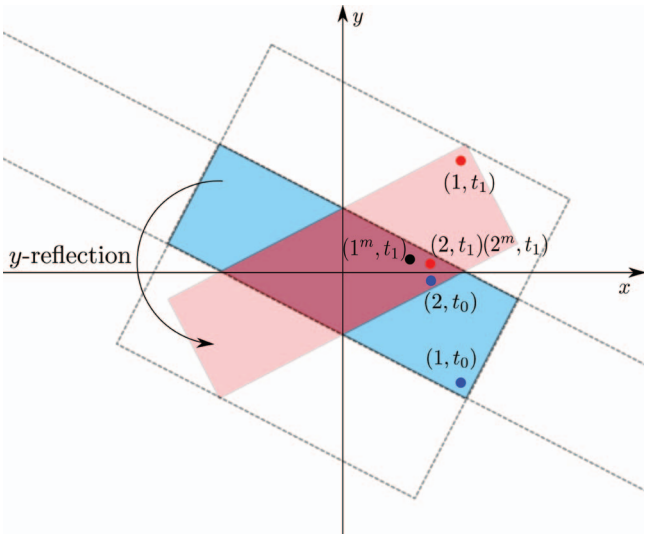

FIG. 1. y-reflection mapping in a rectangular cell oriented by some non-zero angle with respect to the flow fields. The position of two points before mapping is indicated with t_0. After the y-reflection mapping (t_1) and projection onto the initial cell, the relative distance between the points has changed.

require non-orthogonal cells, which makes it very difficult to remap positions without changing the relative distances between atoms and thus disturbing the initial conditions of the flow. Furthermore, the flow field does, in general, not align with the lattice vectors. This can be the case even if a cell is orthogonal, for example, in PEF with the Kraynik-Reinelt periodic boundary conditions.[6]

Figure 1 illustrates the problem that is associated with a phase-space mapping of the coordinates of particles when the cell is not aligned with the cartesian axes. The figure shows a y-reflection mapping[2] in a rectangular cell. The positions of two points before mapping are denoted with $(1, t_0)$ and $(2, t_0)$. The y-reflection mapping reflects the y-coordinates of each point in the cell with respect to the x-axis (i.e., all the positions of the mapped points lie within the red area), and the new positions of the two points are marked by $(1, t_1)$ and $(2, t_1)$. One of the points is still located in the blue cell, whereas the other point is located in a periodic image of the cell. Mapping the periodic images onto the (blue) cell results in the final positions $(1^m, t_1)$ and $(2^m, t_1)$. Relative to the initial points $(1, t_1)$ and $(2, t_1)$, the distance between the two point has changed. Hence, the phase-space mapping in this example interferes with the dynamics of the fluid.

Finding a mapping in which the relative distances between atoms remain unchanged is still an open problem for a simulation cell that is not square or aligned with the field directions. However, the correction shown in Eq. (7), eliminates the need for this specific phase-space mapping. Changing the sign of all of the momenta does not create a phase vector that satisfies the first condition stated above. It does, however, create a distinct phase-space trajectory. Therefore, the time-reversal mapping $\mathbf{\Gamma}_2 = M^T(\mathbf{\Gamma}_1) = (\mathbf{x}, \mathbf{y}, \mathbf{z}, -\mathbf{p}_x, -\mathbf{p}_y, -\mathbf{p}_z)$ is applied to each initial state for the non-equilibrium simulations performed in this study.

In order to obtain good statistics, many non-equilibrium simulations are needed. This is done by running one equilibrium simulation for a long time and branching off many non-equilibrium trajectories. The time between each new set of branches (where each set consists of two branches) is chosen to be larger than the relaxation time of the pressure autocorrelation function in order to make sure that the different sets of branches are uncorrelated to each other.

V. RESULTS AND DISCUSSION

We look at the transient response of the shear stress $B(t) = P_{xy}(t)$ and the normal stresses $B(t) = P_{xx}(t)$, $P_{yy}(t)$ in the plane of deformation. We have chosen to study these stress components since they contribute to the generalized viscosity for PMF.

The nonlinear response is compared to a direct average of the non-equilibrium molecular dynamics simulations, where the average instantaneous pressure tensor is calculated with the virial stress formulation

$$V\mathbf{P}(t) = \left\langle \sum_i \frac{\mathbf{p}_i \mathbf{p}_i}{m} + \frac{1}{2} \sum_{i,j \neq i} \mathbf{F}_{ij}^{\phi} \mathbf{r}_{ij} \right\rangle, \tag{17}$$

where $\mathbf{p}_i \mathbf{p}_i$ denotes the tensor product between the peculiar momentum vectors, $\mathbf{F}_{ij}^{\phi}$ is the interaction force between atoms i and j, and $\mathbf{r}_{ij} = \mathbf{r}_i - \mathbf{r}_j$.

We present simulation results for field strengths, $\dot{\gamma}$ and $\dot{\epsilon}$, 5×10^{-4}, 0.001, 0.005, and 0.05. There is no reason why the shear rate $\dot{\gamma}$ and the elongational rate $\dot{\epsilon}$ should be equal and these values are arbitrarily chosen. Simulations were also run where the shear rate and the elongational rate were not equal (not shown here). These simulations have a different ratio between the shear stress and the normal stress fields, but they show a similar transient behavior. Furthermore, simulations have been run for shear flow and planar elongational flow in order to verify our simulation results with earlier studies.[20,23] Good agreement was found for both types of flow.

Figures 2 and 3 show the stress response under planar mixed flow with $\dot{\epsilon}_{xx} = 0.05$, $\dot{\epsilon}_{yy} = -0.05$, and $\dot{\gamma} = 0.05$. The direct averages of the instantaneous stresses and the TTCF response are shown. The data is averaged over $10 \times 2 \times 7500$ non-equilibrium trajectories, where the first number indicates the number of distinct simulations, the second is the number of simultaneous non-equilibrium trajectories branched off from an equilibrium state (i.e., the original equilibrium starting state and the mapped starting state) and the last number indicates how many pairs of non-equilibrium trajectories are branched off per simulation. Each trajectory is a simulation containing $N = 896$ atoms. The standard error is given by the error bars. The standard error is calculated from the 10 distinct simulations. For this external field, both methods produce smooth, converging profiles which are in good agreement with each other.

For smaller deformation rates, the efficiency of TTCF is expected to become higher than that of direct NEMD averages. Figures 4 and 5 show the transient stress subject to PMF with $\dot{\epsilon}_{xx} = 0.005$, $\dot{\epsilon}_{yy} = -0.005$, and $\dot{\gamma} = 0.005$. The number of non-equilibrium trajectories and the number of atoms are identical to the data shown in Figures 2 and 3. The direct NEMD averages fluctuate strongly around an

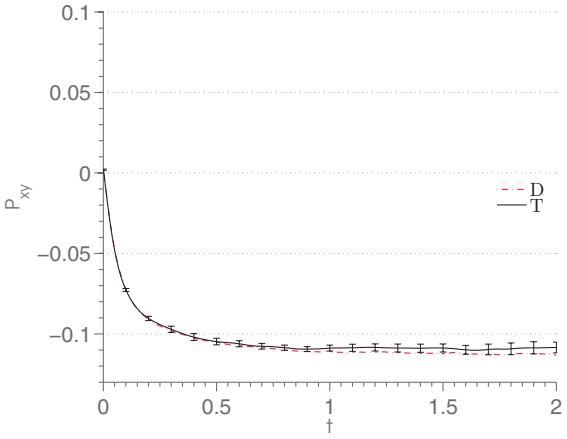

FIG. 2. $B = P_{xy}$ for mixed flow with $\dot{\gamma} = 0.05$ and $\dot{\epsilon} = 0.05$. The label "T" indicates the TTCF result and "D" the direct average over the same non-equilibrium trajectories.

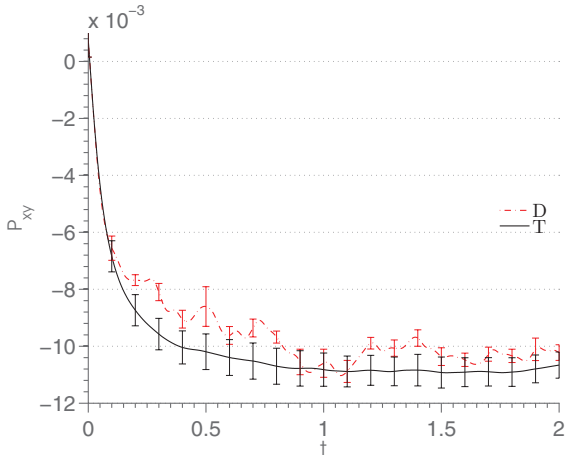

FIG. 4. $B = P_{xy}$ for mixed flow with $\dot{\gamma} = 0.005$ and $\dot{\epsilon} = 0.005$. The label "T" indicates the TTCF result and "D" the direct average over the same non-equilibrium trajectories.

underlying trend, while the TTCF response is again smooth and converges to a steady-state.

One would expect the initial shear stress to be zero and the initial normal stresses equal to the isotropic pressure. In practice, however, the ensemble average is subject to small deviations due to instantaneous fluctuations, as seen in Figures 4 and 5, but converges in the statistical limit of infinitely many atoms or trajectories. As the uncertainty in the ensemble average of the starting states $\langle B(0)\rangle$ is independent of the deformation rate, the relative importance of the initial inaccuracy becomes larger as the external field becomes smaller.

From the transient stresses and the velocity gradient, a "transient viscosity" can be calculated. The viscosity is calculated using the expression presented by Hounkonnou *et al.*[39]

$$\eta(t, \dot{\gamma}, \dot{\epsilon}) = -\frac{\mathbf{\Pi}(t) : \mathbf{S}}{\mathbf{S} : \mathbf{S}}, \tag{18}$$

where $\mathbf{\Pi} = \mathbf{P} - p\mathbf{I}$ is the (traceless) viscous pressure tensor and $\mathbf{S} = \nabla\mathbf{u} + (\nabla\mathbf{u})^{\mathrm{T}}$ is the symmetric strain rate tensor. Hounkonnou *et al.* derived this expression and replaced the viscous stress tensor with the full stress tensor, which in theory gives the same result. In practice, however, this is only the case in the statistical limit due to the uncertainty explained above. We use the formulation where the viscosity follows from the viscous stress, as defined in Eq. (18) above. The steady-state field-dependent viscosity follows from

$$\eta(\dot{\gamma}, \dot{\epsilon}) = \lim_{t\to\infty} \eta(t, \dot{\gamma}, \dot{\epsilon}). \tag{19}$$

Figure 6 shows the viscosity for a mixed flow with $\dot{\gamma} = 0.005$ and $\dot{\epsilon} = 0.005$. The TTCF response clearly converges to the steady-state viscosity $\eta = 2.35 \pm 0.02$, whereas the direct average (calculated from the same number of trajectories) remains noisy. The viscosity calculated from a steady-state long time-average at the same state point and with the same deformation rate is $\eta = 2.31 \pm 0.09$, which is in good agreement with the TTCF result.

The results shown in Figures 7 and 8 illustrate, for a mixed flow with $\dot{\gamma} = 0.001$ and $\dot{\epsilon} = 0.001$, that the statistical inaccuracy of $\langle B(0)\rangle$ becomes relatively important for very small fields, where the response is small. While the response to the field at $t > 0$ is very accurate for weak fields,

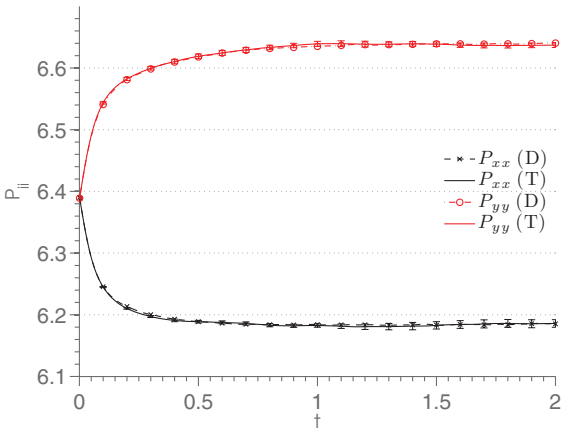

FIG. 3. Normal stress response under planar mixed flow with $\dot{\epsilon}_{xx} = 0.05$, $\dot{\epsilon}_{yy} = -0.05$, and $\dot{\gamma} = 0.05$. The label "T" indicates the TTCF result and "D" the direct average over the same non-equilibrium trajectories.

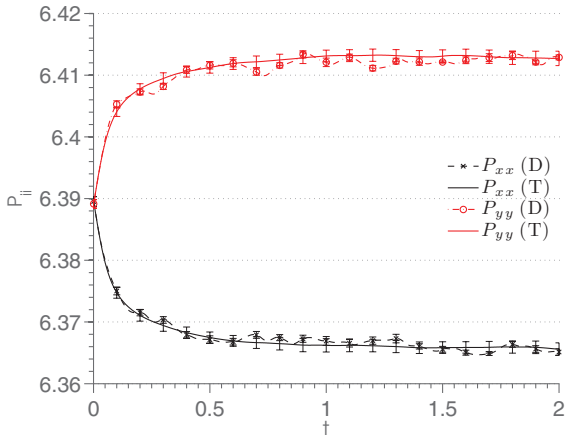

FIG. 5. Normal stress response under planar mixed flow with $\dot{\epsilon}_{xx} = 0.005$, $\dot{\epsilon}_{yy} = -0.005$, and $\dot{\gamma} = 0.005$. The label "T" indicates the TTCF result and "D" the direct average over the same non-equilibrium trajectories.

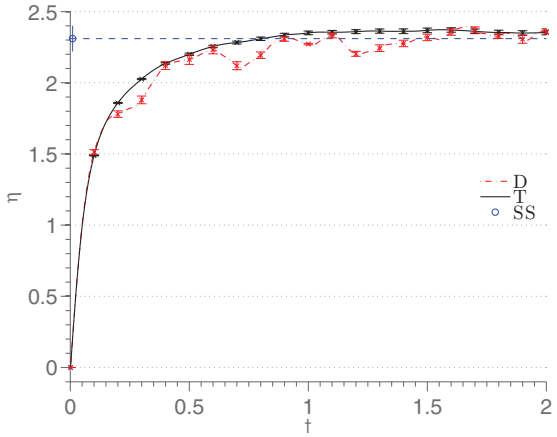

FIG. 6. Viscosity for mixed flow with $\dot{\gamma} = 0.005$ and $\dot{\epsilon} = 0.005$. The label "T" indicates the TTCF result, "D" the direct NEMD average and "SS" is the viscosity calculated from a steady-state time-average of a different simulation at the same state point.

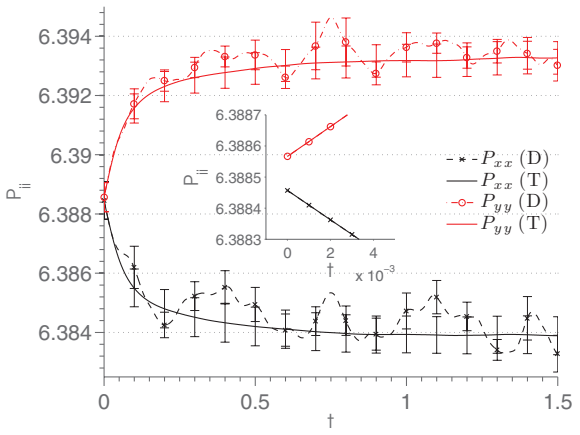

FIG. 8. Normal stress response under planar mixed flow with $\dot{\epsilon}_{xx} = 0.001$, $\dot{\epsilon}_{yy} = -0.001$, and $\dot{\gamma} = 0.001$. The label "T" indicates the TTCF result and "D" the direct NEMD average. The inset shows the normal stresses directly after the external field is activated. The error bars are not shown in the inset, since they are too large to fit in the domain shown.

the error in the initial $t = 0$ ensemble implies an error in the trajectory origin. The figures show that the magnitude of the error bars remains approximately constant in time, meaning that the initial error in $\langle B(0)\rangle$ (at equilibrium) dominates the uncertainty for all time. The inset in Figure 8 shows that the equilibrium value ($t = 0$) of both normal stresses are not identical. Similarly, Figure 7 shows that the initial shear stress is non-zero due to numerical inaccuracy. In the case of $B = P_{xy}$, we know that the initial value should be zero, and for the normal stresses we know that in the thermodynamic limit $P_{xx}(0) = P_{yy}(0) = P_{zz}(0) = p = \frac{1}{3}\mathrm{Tr}(\mathbf{P})$ has to apply. However, a generic approach to eliminate the uncertainty of the direct averages $\langle B(0)\rangle$ is unknown. Note that the viscosity calculation does not suffer from this inaccuracy, since only the viscous stresses are taken into account. The viscosity calculated for a mixed flow with $\dot{\gamma} = 0.001$ and $\dot{\epsilon} = 0.001$ converges to $\eta = 2.31 \pm 0.01$, which is slightly lower than the viscosity calculated for a field $\dot{\gamma} = 0.005$ and $\dot{\epsilon} = 0.005$.

For an even smaller field, the numerical uncertainty in the starting states of the trajectories becomes even more dominant. To illustrate the difference with the stress fields shown previously, Figures 9 and 10 show the viscous stresses for a mixed flow with $\dot{\gamma} = 5 \times 10^{-4}$ and $\dot{\epsilon} = 5 \times 10^{-4}$. The number of atoms is again $N = 896$ and the number of trajectories used is now $10 \times 2 \times 20\,000$. Considering only the viscous stresses clearly shows the difference in quality between the direct averages and TTCF. The standard deviation for the direct averages is large relative to the response, whereas TTCF results in a smooth profile with a high accuracy. The viscosity converges to $\eta = 2.28 \pm 0.01$, which is again slightly lower than the viscosity calculated for a field $\dot{\gamma} = 0.001$ and $\dot{\epsilon} = 0.001$. The direct averaged stress fields are much too noisy to calculate a meaningful viscosity.

For these small fields, the nonlinearity of the response of the atomic fluid becomes negligibly small and the viscosity approaches the Newtonian regime. In this regime, the

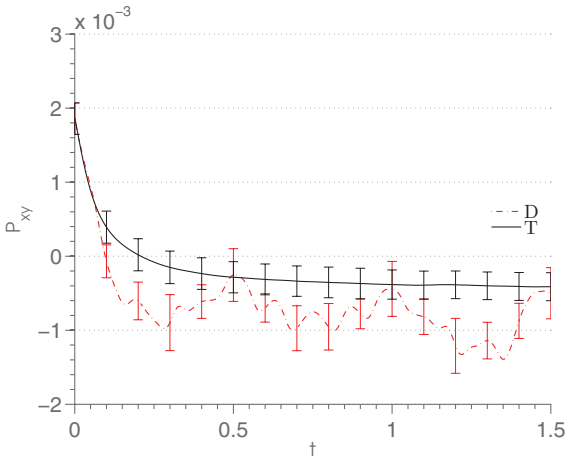

FIG. 7. $B = P_{xy}$ for mixed flow with $\dot{\gamma} = 0.001$ and $\dot{\epsilon} = 0.001$. The label "T" indicates the TTCF result and "D" the direct NEMD average. The error in the starting point of the trajectory is of the same order of magnitude as the response.

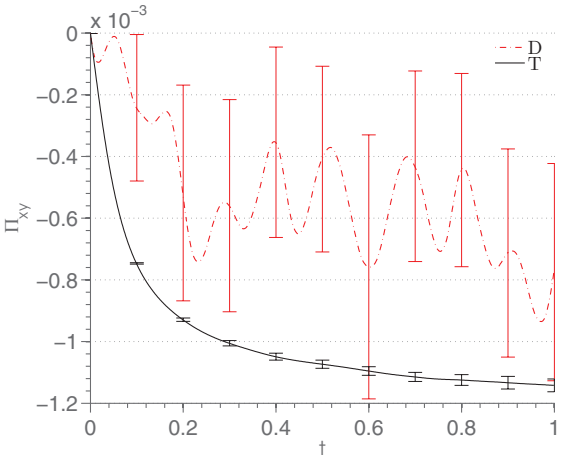

FIG. 9. Viscous shear stress Π_{xy} for mixed flow with $\dot{\gamma} = 5 \times 10^{-4}$ and $\dot{\epsilon} = 5 \times 10^{-4}$. The label "T"indicates the TTCF result and "D" the direct average over the same non-equilibrium trajectories. The number of trajectories used is $10 \times 2 \times 20\,000$.

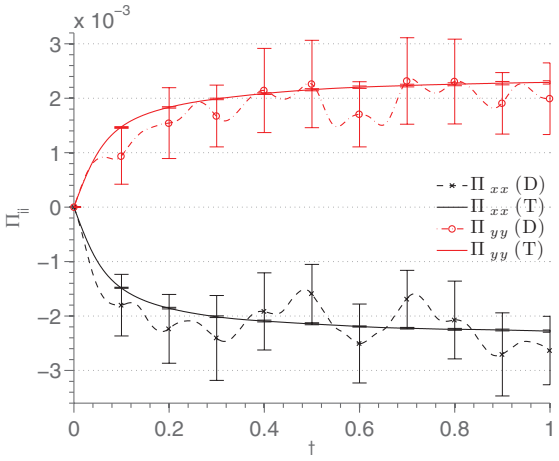

FIG. 10. Viscous normal stress response under planar mixed flow with $\epsilon = 5 \times 10^{-4}$ and $\dot{\gamma} = 5 \times 10^{-4}$. The label "T" indicates the TTCF result and "D" the direct average over the same non-equilibrium trajectories. The number of trajectories used is $10 \times 2 \times 20\,000$.

transport properties are independent of the external field, thus simulations are suitable for comparison to experiments on simple Newtonian fluids.

VI. CONCLUSIONS

We have applied TTCF to atomic PMF for a variety of small fields strengths. We have presented the stress response and viscosities both in the shear-thinning region and in the Newtonian region. Good agreement was found between direct averages of NEMD simulations and the TTCF response for relatively large field strengths. For small field strengths, the direct averages show a decrease in the accuracy of the calculation, whereas the accuracy in the TTCF response is invariant to changes in the field strength. TTCF proves to be far more efficient at small deformation rates than direct averages of NEMD simulations. Therefore, this method can be applied to fluids with deformation rates which are much smaller than those commonly used in NEMD simulations and thus approach the field strengths that are typical in experiments.

We have shown that by subtracting the known error from the correlation function, special phase-space mappings are not required. Without the need for phase-space mappings, it becomes possible to apply TTCF, with a high accuracy, to each type of homogeneous flow that can be simulated for an indefinitely long time, for example, elliptical flows. This is merely one of the yet unexplored applications for TTCF.

While this study presents the application of TTCF to atomic PMF, the methods discussed here are more generally applicable. Applying the theories discussed in this study to molecular fluids, bridges the gap between molecular dynamics simulations and industrial applications and allows for a direct comparison between both.

ACKNOWLEDGMENTS

R.H. would like to acknowledge the support of Professor Stefan Luding and the financial support of NWO-STW VICI grant No. 10828 and MicroNed grant 4-A-2.

[1] D. J. Evans and G. P. Morriss, Phys. Rev. A **30**, 1528 (1984).
[2] D. J. Evans and G. P. Morriss, *Statistical Mechanics of Nonequilibrium Liquids* (Cambridge University Press, New York, 2008).
[3] P. J. Daivis and B. D. Todd, J. Chem. Phys. **124**, 194103 (2006).
[4] B. D. Todd and P. J. Daivis, Mol. Simul. **33**, 189 (2007).
[5] A. W. Lees and S. F. Edwards, J. Phys. C **5**, 1921 (1972).
[6] A. M. Kraynik and D. A. Reinelt, Int. J. Multiphase Flow **18**, 1045 (1992).
[7] B. D. Todd and P. J. Daivis, Phys. Rev. Lett. **81**, 1118 (1998).
[8] B. D. Todd and P. J. Daivis, Comput. Phys. Commun. **117**, 191 (1999).
[9] A. Baranyai and P. T. Cummings, J. Chem. Phys. **110**, 42 (1999).
[10] A. Dua and B. J. Cherayil, J. Chem. Phys. **119**, 5696 (2003).
[11] E. S. G. Shaqfeh, J. Non-Newtonian Fluid Mech. **130**, 1 (2005).
[12] T. A. Hunt, S. Bernardi, and B. D. Todd, J. Chem. Phys. **133**, 154116 (2010).
[13] B. R. Bird and O. Hassager, *Dynamics of Polymeric Liquids, Fluid Mechanics* (Wiley-Interscience, New York, 1987), Vol. 1.
[14] S. Bair, C. McCabe, and P. T. Cummings, Phys. Rev. Lett. **88**, 058302 (2002).
[15] E. G. D. Cohen, Phys. A **118**, 17 (1983).
[16] J. W. Dufty and M. J. Lindenfeld, J. Stat. Phys. **20**, 259 (1979).
[17] G. Pan and C. McCabe, J. Chem. Phys. **125**, 194527 (2006).
[18] O. A. Mazyar, G. Pan, and C. McCabe, Mol. Phys. **107**, 1423 (2009).
[19] G. P. Morriss and D. J. Evans, Phys. Rev. A **35**, 792 (1987).
[20] D. J. Evans and G. P. Morriss, Phys. Rev. A **38**, 4142 (1988).
[21] I. Borzsák, P. T. Cummings, and D. J. Evans, Mol. Phys. **100**, 2735 (2002).
[22] C. Desgranges and J. Delhommelle, J. Chem. Phys. **128**, 084506 (2008).
[23] B. D. Todd, Phys. Rev. E **56**, 6723 (1997).
[24] B. D. Todd, Phys. Rev. E **58**, 4587 (1998).
[25] D. J. Evans and G. P. Morriss, Chem. Phys. **87**, 451 (1984).
[26] G. P. Morriss and D. J. Evans, Mol. Phys. **54**, 629 (1985).
[27] P. T. Cummings and D. J. Evans, Ind. Eng. Chem. Res. **31**, 1237 (1992).
[28] D. J. Evans and G. P. Morriss, Phys. Rev. Lett. **51**, 1776 (1983).
[29] T. A. Hunt and B. D. Todd, J. Chem. Phys. **131**, 054904 (2009).
[30] C. Desgranges and J. Delhommelle, Mol. Simul. **35**, 405 (2009).
[31] D. M. Heyes, Chem. Phys. **98**, 15 (1985).
[32] V. Kalra and Y. L. Joo, J. Chem. Phys. **131**, 214904 (2009).
[33] C. Baig, B. Jiang, B. J. Edwards, D. J. Keffer, and H. D. Cochran, J. Rheol. **50**, 625 (2006).
[34] P. J. Daivis, M. L. Matin, and B. D. Todd, J. Non-Newtonian Fluid Mech. **111**, 1 (2003).
[35] P. J. Daivis, M. L. Matin, and B. D. Todd, J. Non-Newtonian Fluid Mech. **147**, 35 (2007).
[36] M. W. Evans and D. M. Heyes, Mol. Phys. **69**, 241 (1990).
[37] J. D. Weeks, D. Chandler, and H. C. Andersen, J. Chem. Phys. **54**, 5237 (1971).
[38] D. J. Evans, W. G. Hoover, B. H. Failor, B. Moran, and A. J. C. Ladd, Phys. Rev. A **28**, 1016 (1983).
[39] M. N. Hounkonnou, C. Pierleoni, and J. P. Ryckaert, J. Chem. Phys. **97**, 9335 (1992).